

# Review and Comments for the Development of Point Defect-Controlled CZ-Si Crystals and Their Application to Future Power Devices

*Masataka Hourai,\* Toru Nagashima, Hideshi Nishikawa, Wataru Sugimura, Toshiaki Ono, and Shigeru Umeno*

**Development of point defect-controlled Czochralski silicon (CZ-Si) crystal growth technology by v/G control, i.e., the ratio of growth rate (v) to the axial temperature gradient (G) in the crystal near its melting point, is reviewed and nitrogen- and hydrogen-doping technologies are proposed for 300-mm magnetic-field-applied CZ-Si (MCZ-Si) crystals free of grown-in defects with very low oxygen for application to future silicon power devices such as insulated gate bipolar transistors (IGBTs). Using a hot zone with a uniform G distribution in a crystal radial direction, v/G is maintained by controlling v of around the critical value at which the amount of vacancies is balanced with that of self-interstitials so that the generation of grown-in defects, such as voids and dislocation clusters, are suppressed. Nitrogen-doping or hydrogen-doping technology combined with v/G control also enables the enlarging of the process window for grown-in defect-free MCZ-Si crystals that can be used as an alternative material to floating zone-Si crystals. The advantages and disadvantages of both technologies are discussed from the view point of crystal quality required to guarantee higher performance of future IGBTs.**

been achieved in silicon-crystal-growth technology, which has been providing the base material supporting the progress of semiconductor devices.<sup>[1–3]</sup> From the year 2000 onward, 300-mm grown-in defect-free Czochralski silicon (CZ-Si) crystals have been mass-produced by precisely controlling point defects during crystal growth.<sup>[4,5]</sup> In this paper, we review the development of point-defect-controlled CZ-Si crystal growth technology and discuss the technical issues with developing 300-mm magnetic-field-applied CZ-Si (MCZ-Si) crystals for application to future silicon power devices, especially insulated gate bipolar transistors (IGBTs).

## 2. Development of Point-Defect-Controlled CZ-Si Crystals

### 2.1. Brief History of Research on Grown-In Defects in CZ-Si Crystals

In 1989 and 1990, two important findings were reported with regard to an oxidation-induced stacking fault-ring (OSF-ring) appearing in CZ-Si crystals. Hasebe et al.<sup>[6]</sup> first showed that the OSF-ring shrinks from the crystal periphery and disappears at the center with a reduction in the crystal pulling rate. Tachimori et al.<sup>[7]</sup> then found that the gate oxide integrity (GOI) characteristics of metal oxide semiconductor (MOS) diodes significantly differ inside and outside the OSF-ring, i.e., the GOI yield is excellent outside the ring while poor inside the ring. As these findings attracted strong interest, within a few years several types of grown-in defects, such as laser scattering tomography defects (LSTDs),<sup>[8,9]</sup> flow pattern defects (FPDs),<sup>[10]</sup> and Secco etch pit defects (SEPDs),<sup>[9]</sup> and crystal originated particles (COPs),<sup>[11]</sup> were found to exist inside the OSF-ring by using different detection methods. They were independently confirmed to correlate well with the GOI characteristics.

Since then, to improve the crystal quality satisfying the requirements of advanced devices, the nature and formation behavior and techniques to control grown-in defects have been extensively investigated. As a result, grown-in defects have been reduced from densities of about  $10^6$  or above to those of about

## 1. Introduction

Along with the remarkable progress in semiconductor devices over the past half a century, many significant improvements have

---

Dr. M. Hourai  
Technology Division  
SUMCO Corporation  
1-52 Kubara, Yamashiro-cho, Imari, Saga 849-4256, Japan  
E-mail: mhourai@sumcosi.com

T. Nagashima, H. Nishikawa  
Customer Product Engineering Department  
Technology Division  
SUMCO Corporation  
2201 Oaza Kamioda, Kohoku-machi, Kishima-gun, Saga 849-0597,  
Japan

Dr. W. Sugimura, Dr. T. Ono, Dr. S. Umeno  
Advanced Evaluation and Technology Department  
Technology Division  
SUMCO Corporation  
1-52 Kubara, Yamashiro-cho, Imari, Saga 849-4256, Japan

 The ORCID identification number(s) for the author(s) of this article can be found under <https://doi.org/10.1002/pssa.201800664>.

DOI: 10.1002/pssa.201800664

$10^5 \text{ cm}^{-3}$  or below due to the optimization of the thermal histories of crystals during growth.<sup>[12–14]</sup> Umeno et al.<sup>[15]</sup> confirmed that LSTDs existing inside the OSF-ring are the same as FPDs and COPs. LSTDs were also identified to be octahedral voids through direct observation using transmission electron microscopy (TEM).<sup>[16–18]</sup> Sadamitsu et al.<sup>[9]</sup> also confirmed that dislocation clusters due to self-interstitials exist outside the OSF-ring.

However, in spite of such intensive efforts, in the late 1990s, many device manufacturers began to consider adopting epitaxial wafers instead of polished CZ-Si wafers. The major reason for this is that grown-in defects affected advanced devices during that time due to reducing the feature-size of devices to that of grown-in defects ( $\approx 100 \text{ nm}$ ).<sup>[19,20]</sup> To continue using polished CZ-Si wafers in advanced devices under such circumstances, it is necessary to fabricate grown-in defect-free wafers having crystal quality equivalent to that of epitaxial wafers.

## 2.2. Growth Parameter for Determining Defect Type in CZ-Si Crystals

In floating zone (FZ)-Si crystals, the change in the grown-in defects from A and/or B swirl to D defects was also known to occur depending on the crystal growth rate.<sup>[21]</sup> Voronkov<sup>[22]</sup> pointed out that the change in the defect type in FZ-Si crystals occurs at a critical value of  $v/G$ ; ratio of the growth rate ( $v$ ) to the axial temperature gradient ( $G$ ) at the solid/liquid interface, hereafter we use  $v$  as a crystal pulling rate for CZ-Si. However, the parameters affecting the behavior of grown-in defects, such as voids and dislocation clusters, in CZ-Si crystals were unknown except for the pulling rate, as described above. Hence, we investigated the behavior of grown-in defects by changing the parameters affecting the temperature distribution in a growing crystal.

### 2.2.1. Experimental

To change the temperature distribution in a growing crystal, four different hot zones, i.e., I–IV, as shown in **Table 1** and **Figure 1(a)**, were used in a CZ furnace with a 16-inch diameter crucible.<sup>[23]</sup> To change the hot zones, two parameters were adjusted (1) melt position; the position of the silicon melt surface measured from the top of the heater and (2) shield-melt gap; the gap between the melt surface and lower end of the



**Masataka Hourai** received B.S. and M.S. degrees in physical chemistry and inorganic chemistry from Osaka University, Japan, in 1980 and 1982. He subsequently joined the Semiconductor Research Lab. at Matsushita Electric Industrial before joining SUMCO Corp., Japan, in 1985. His research interest is in defects in Si and he developed several types of CZ-Si crystals and wafers. He received Dr. of Eng. in Material and Life Science from Osaka University in 1996. He held the position of general manager of the Advanced Technology Development Dept. and Analysis & Characterization Technology Dept. at SUMCO and is currently a senior professional engineer in the Technology Division.

radiation shield, as shown in **Figure 1(a)**. These parameters affect the amount of radiation heat flux into a growing crystal from the heater and silicon melt. Thirteen 150-mm-diameter, B-doped (resistivity  $4.5\text{--}6 \Omega \text{ cm}$ ),  $<100>$ -oriented, CZ-Si crystals with oxygen concentrations of about  $15\text{--}18 \times 10^{17} \text{ atoms cm}^{-3}$  (ASTM F-121, 1979) were grown under the growth conditions shown in **Table 1**. Sample wafers were cut parallel or perpendicular to the growth axis, and the macroscopic distribution of grown-in defects was evaluated by the characteristic oxygen precipitation pattern observed using X-ray topography after 2-step annealing ( $800^\circ\text{C}/4\text{ h} + 1000^\circ\text{C}/16\text{ h}$  in  $\text{O}_2$ ). LSTDs, FPDs and large dislocation pits were observed in the as-grown state by infrared (IR) tomography and Secco etching, respectively. X-ray topography images were also taken after Cu-decoration ( $900^\circ\text{C}/20\text{ min}$  in  $\text{N}_2$ ) or high-temperature oxidation ( $1150^\circ\text{C}/8\text{ h}$  in  $\text{O}_2$ ).

The temperature distributions of all crystals were calculated using the global heat transfer model.<sup>[24]</sup> As the effect of the melt convection was not taken into account in this calculation, the calculated shape of the solid/liquid interface was different from the actual shape. To obtain a more accurate temperature distribution near the interface, the actual shape of the interface was measured from X-ray topography images after 2-step annealing. Using the measured interface shape and the temperatures at the crystal surface calculated from the global heat transfer model, the modified temperature distribution in

**Table 1.** Experimental conditions.<sup>[23]</sup>

Hot zone	Melt position [mm]	Shield-melt gap [mm]	Charge weight [kg]	Pulling rate [ $\text{mm min}^{-1}$ ]
I	–50	40	35	0.40, 0.65, 0.95
II	–50	80	35, 45 <sup>a)</sup>	0.40, 0.65 <sup>a)</sup> , 0.80
III	–90	40	35	0.40, 0.65, 0.85
IV	–90	80	35	0.40, 0.65, 0.75

<sup>a)</sup> The exceptional crystal grown with non-standard charge weight of 45 kg and pulling rate of  $0.65 \text{ mm min}^{-1}$ .

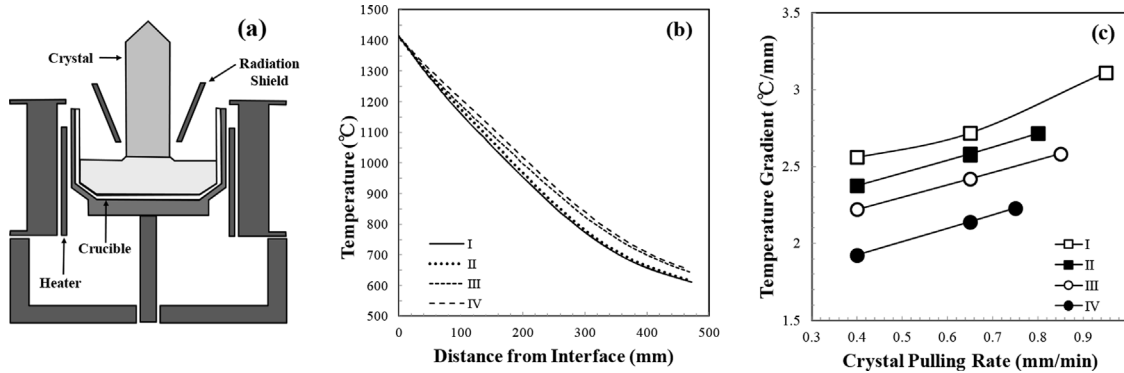


**Figure 1.** a) Schematic of CZ furnace, (b) calculated axial temperature distributions up to 400 mm in length for crystals grown in hot zones I–IV with pulling rate of  $0.65 \text{ mm min}^{-1}$ , and (c) axial temperature gradients as function of crystal pulling rate. Adapted with permission.<sup>[23]</sup> Copyright 1995, Trans Tech Publications Ltd.

the crystals was calculated using commercially available software (ABAQUS).

Figure 1(b) shows the calculated axial temperature distributions up to 400 mm in length for crystals grown in each hot zone with a pulling rate of  $0.65 \text{ mm min}^{-1}$ . The axial temperature gradient decreased in the order of hot zones I–IV. Figure 1(c) shows the axial temperature gradients for crystals grown in each hot zone as a function of the crystal pulling rate, where the temperature gradients were averaged between 1400 and  $1300^\circ\text{C}$ . The temperature gradients in crystals for each hot zone were found to increase with increasing crystal pulling rate.

#### 2.2.2. Relationship Between OSF-Ring Diameter and $v/G$

Figure 2 show X-ray topography images taken after 2-step annealing ( $800^\circ\text{C}/4\text{ h} + 1000^\circ\text{C}/16\text{ h in O}_2$ ) for crystals grown in each hot zone with a pulling rate of  $0.65 \text{ mm min}^{-1}$ . Although the crystals were grown with the same pulling rate, the OSF-ring did not appear at the same radial position, and the OSF-ring radius varied in the growth direction. With decreasing temperature gradient, as observed in hot zones I–IV, the OSF-ring position moved toward the crystal periphery. When the OSF-ring shrank to as small as about half the crystal radius, a region with dislocation clusters appeared outside the OSF-ring, as observed in the crystal grown in hot zones I.

Figure 3(a) and (b) show X-ray topography images after 2-step annealing for crystals grown at maximum pulling rates of  $0.95$  and  $0.75 \text{ mm min}^{-1}$  in hot zones I with the largest G and the hot zone IV with the smallest G, respectively. Figure 3(c) and (d) also show the images for crystals grown at minimum pulling rate of  $0.4 \text{ mm min}^{-1}$  in hot zones I and IV, respectively. As shown in Figure 3(a), the OSF-ring was distributed in the peripheral area of the crystal except for the top part. However, as shown in Figure 3(b), the OSF-ring distributed more in the outer periphery of the crystal than that in Figure 3(a). On the other hand, as shown in Figure 3(c), when the crystal was grown in the hot zone I with the largest G at the minimum pulling rate of  $0.4 \text{ mm min}^{-1}$ , dislocation clusters occurred in all parts of the crystal. However, as shown in Figure 3(d), in the crystal grown at the

minimum pulling rate of  $0.4 \text{ mm min}^{-1}$  in hot zone IV with the smallest G, an extraordinary defect distribution was observed. More specifically, a transformation of defect regions from the dislocation cluster to the void through the OSF-ring, which generally occurs in the top part of the crystal as clearly seen in Figure 3(a), was observed to be stretched over almost the entire body of the crystal. This crystal will be discussed in more detail in a later section.

Figure 4(a) shows the relationship between OSF-ring position and pulling rate at the axial positions 100, 200, 300, and 400 mm of crystals grown in each hot zone. The OSF-ring diameter was reduced by reducing the crystal pulling rate, but these trends differed depending on the hot zone, i.e., the larger the G was, the faster the OSF-ring diameter shrunk. Figure 4(b) shows the relationship between the OSF-ring diameter and  $v/G$ . It was found that the OSF-ring diameter can be normalized by  $v/G$  without depending on the hot-zone and crystal axial position.<sup>[23,25]</sup>

In the case of a large  $v/G$ , the OSF-ring is distributed in the outer periphery of the crystal and voids due to vacancies appear inside the OSF-ring. With a reduction in  $v/G$ , the OSF-ring shrinks and disappears at the center of the crystal at a critical  $v/G$  of about  $0.22 \text{ mm}^2 (\text{°C min})^{-1}$ . Furthermore, when  $v/G$  is below the critical value, dislocation clusters due to self-interstitials occur over the entire area of the crystal. A similar relationship was also reported by Von Amon et al.<sup>[26]</sup> Therefore, it was concluded that  $v/G$  is the growth parameter determining the type of grown-in defects appearing in CZ-Si crystals, which is similar to the case in FZ-Si crystals.<sup>[22]</sup>

At high temperatures near the melting point in a growing CZ-Si crystal, diffusion and recombination processes of point defects occur, so a distribution of point defects is determined by  $v/G$  in the same manner as FZ-Si. However, during the subsequent cooling process, grown-in defects that differ from those of FZ-Si may form by the interaction of point defects with super-saturated oxygen in CZ-Si crystals. Such behavior of point defects during CZ-Si crystal growth was explained in many studies conducted in the 1990s<sup>[27–31]</sup> by using the up-hill diffusion model proposed by Habu et al.<sup>[32–35]</sup> However, an explanation by using the Voronkov's model is now widely accepted.<sup>[22]</sup>

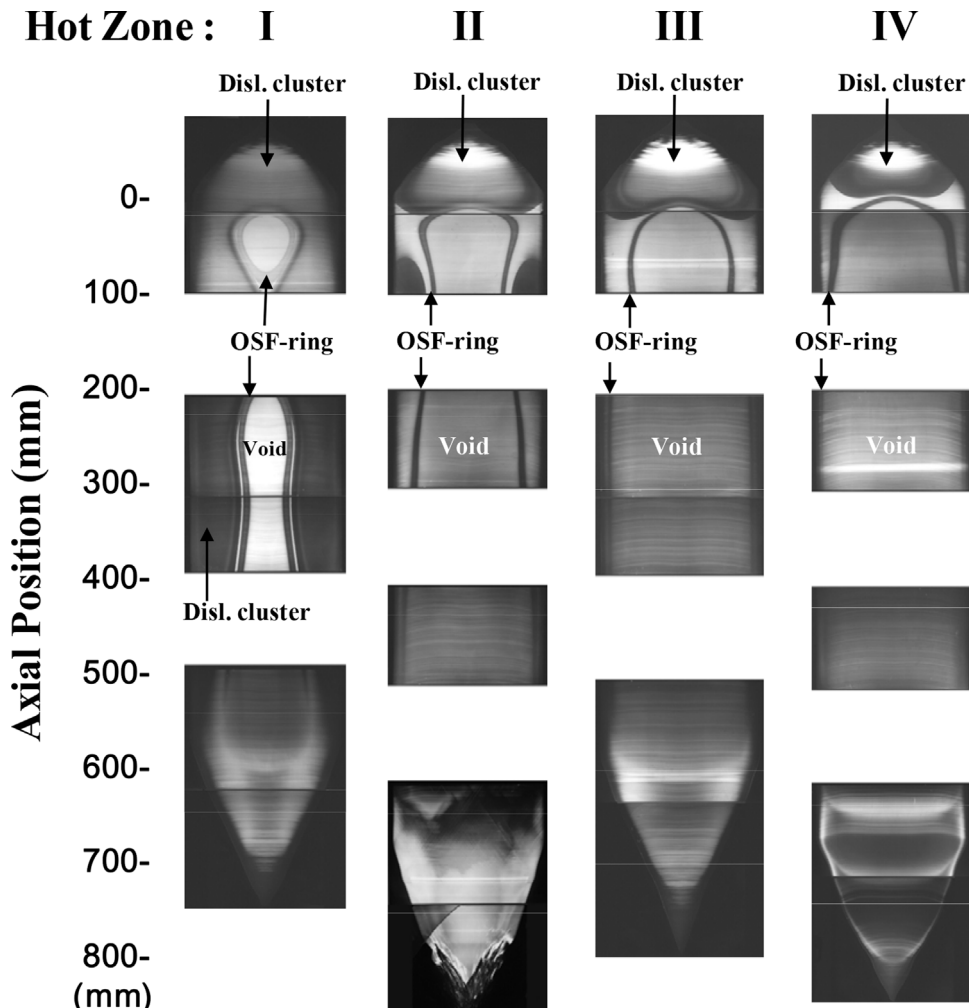


**Figure 2.** X-ray topography images taken after 2-step annealing for crystals grown in hot zones I–IV with pulling rate of  $0.65 \text{ mm min}^{-1}$ . Adapted with permission.<sup>[30]</sup> Copyright 1998, Electrochemical Society.

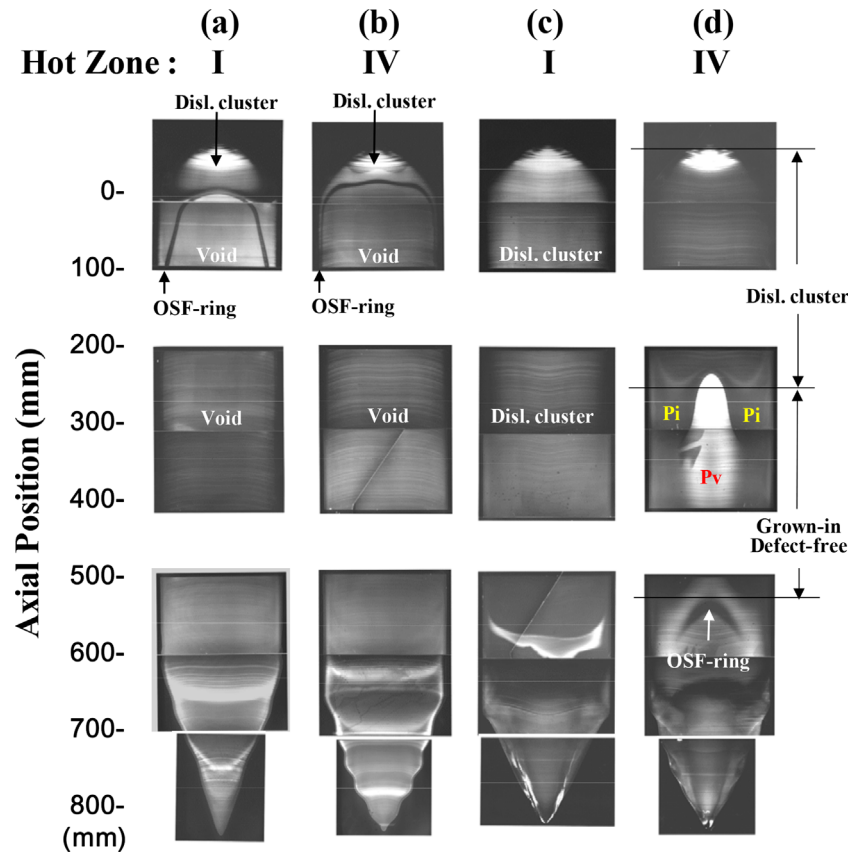
### 2.2.3. Relationship Between Radial Distribution of Grown-In Defects in CZ-Si Crystal and $\nu/G$

Figure 5(a)–(c) show X-ray topography images of the top part of the crystal grown in hot zone II with  $\nu = 0.65 \text{ mm min}^{-1}$  and charge weight of 45 kg after (a) Cu-decoration, (b)  $1150^\circ\text{C}/8 \text{ h}$  in  $\text{O}_2$  oxidation, and (c) the 2-step annealing. Figure 5(d) shows the radial distributions of LSTDs observed using IR tomography, FPDs, large dislocation pits observed after Secco etching, OSF observed after Wright etching, and bulk micro defects (BMDs) observed using IR tomography after high-temperature oxidation at  $1150^\circ\text{C}/8 \text{ h}$ . These defects were observed at the axial position denoted with the arrow in Figure 5(c). As shown by the letters A–D in Figure 5(c), the CZ-Si crystal can be divided into four defect regions from the characteristic of the grown-in defects.

In region C (inside the OSF-ring), LSTDs and FPDs were observed in the as-grown state, and their densities and size increased with increasing distance from the OSF-ring. LSTDs

and FPDs are voids formed by the aggregation of super-saturated vacancies in a narrow temperature range from around  $1100^\circ\text{C}$  to about  $30^\circ\text{C}$  in the cooling process after crystal solidification.<sup>[36,37]</sup> Their formation temperature depends on the vacancy super-saturation just before aggregation in the growing crystal.<sup>[38]</sup> As the vacancy super-saturation increases, the void-formation temperature becomes higher; hence, their sizes become larger due to the increase in the void growth rate. The size of LSTDs observed in region C were relatively large near the crystal center and became smaller toward the OSF-ring. Therefore, super-saturation of vacancies in region C is relatively high at the crystal center and decreases toward the OSF-ring. In the case of the OSF-ring being about half the crystal radius or smaller, the size of LSTDs was observed to be markedly small. This fact implies that the shrinkage of the OSF-ring results from the lowering of vacancy super-saturation.

In region B (the OSF-ring region), no defects were observed in the as-grown state; however, a high density of defects were



**Figure 3.** X-ray topography images after 2-step annealing for crystals grown with (a) and (b) maximum pulling rates in hot zones I and IV and (c) and (d) minimum pulling rate of  $0.4 \text{ mm min}^{-1}$  in hot zones I and IV, respectively.

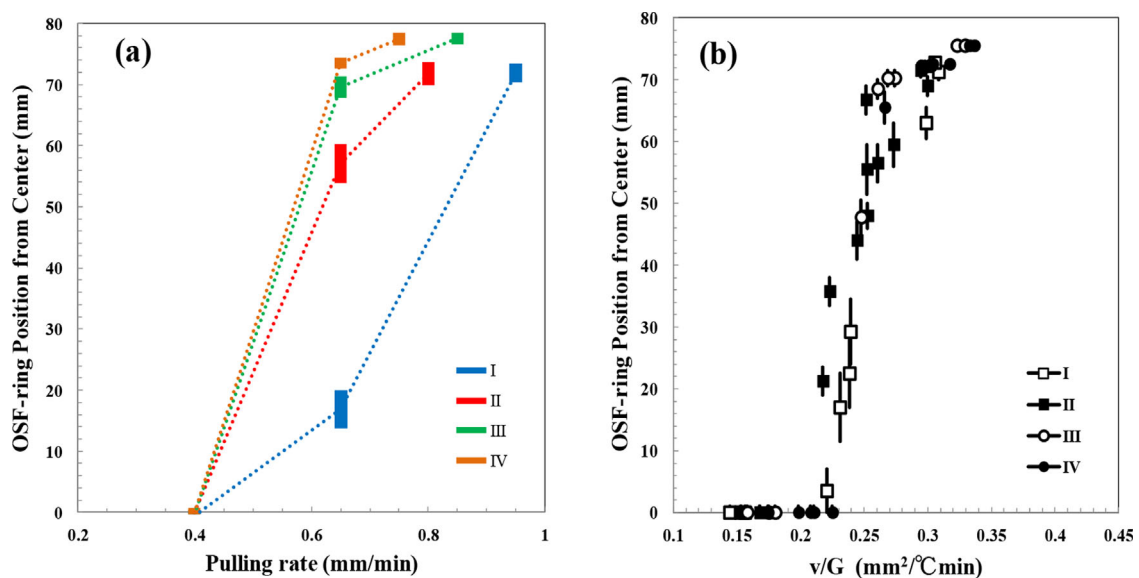


**Figure 4.** OSF-ring radius at axial positions of 100, 200, 300, 400 mm and other characteristic positions of crystals grown in each hot zone as functions of (a) pulling rate and (b)  $v/G$ . Adapted with permission.<sup>[23]</sup> Copyright 1995, Trans Tech Publications Ltd.

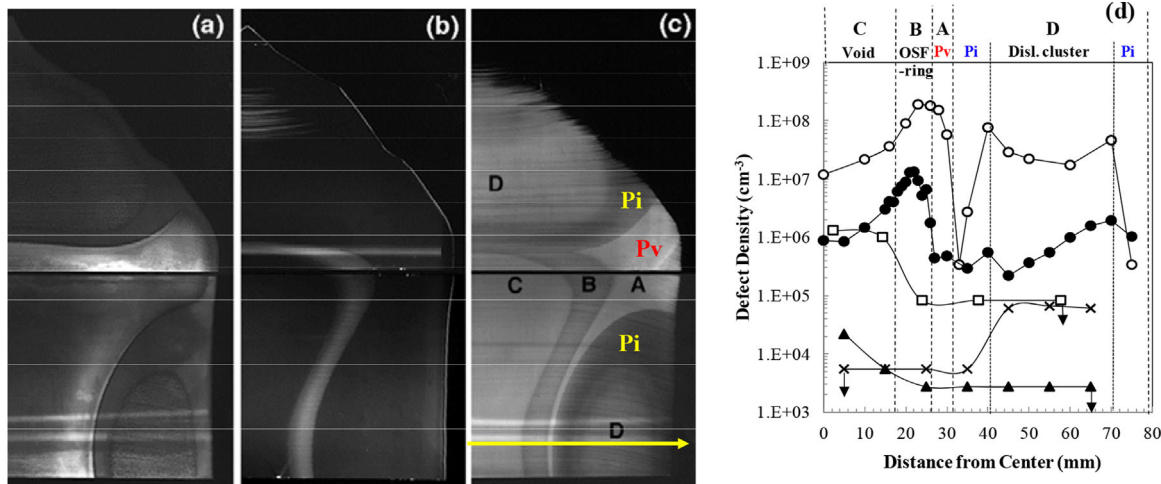


**Figure 5.** X-ray topography images taken after (a) Cu-decoration, (b) high-temperature oxidation at 1150 °C, and (c) 2-step annealing for top part of crystal grown in hot zone II with 45-kg poly-Si charge and pulling rate of 0.65 mm min<sup>-1</sup>. d) Radial distributions of grown-in defects; □ IR-LSTDs, ▲ PFDs, × large pit due to dislocation cluster, and ● OSF and ○ BMD distributions after oxidation at 1150 °C observed at radial position denoted with arrow in (c). Arrows in (d) show detection limits. Adapted with permission.<sup>[23]</sup> Copyright 1995, Trans Tech Publications Ltd.

observed after Cu-decoration, as shown in Figure 5(a). In addition, oxygen precipitates with a density of about 10<sup>8</sup> cm<sup>-3</sup> and OSF with a density of about 10<sup>7</sup> cm<sup>-3</sup> was observed after high-temperature oxidation at 1150 °C, as shown in Figure 5(b) and (d). Some of these oxygen precipitates have been reported to act as nuclei for OSF formation.<sup>[39]</sup> Therefore, the grown-in defects existing in region B are not large enough to be detectable in the as-grown state; however, they are very stable oxygen-precipitate nuclei able to grow even at high temperatures ( $\leq 1250$  °C). These nuclei have been reported to form during crystal growth at medium temperatures from 1020 to 850 °C.<sup>[40]</sup> Therefore, it is suggested that vacancies are also the dominant point defects existing in region B; however, super-saturation is lower than that in region C.

In region A (just outside the OSF-ring), no defects were observed in the as-grown state, but a high density of defects were observed after Cu-decoration in a manner similar to that of region B. In addition, strong oxygen precipitation was observed after the 2-step annealing. Therefore, it was inferred that these precipitation nuclei in region A form due to a small number of vacancies remained without consumption for void formation. Therefore, region A is a vacancy-type grown-in defect-free region.

Region D (outside region A) can be divided into two sub-regions, as is shown in Figure 5(a) and (c). In the central area of region D, striated defects were visualized after Cu-decoration. Large dislocation pits were also observed by Secco etching, and these pits were identified as dislocation clusters by using the TEM.<sup>[9]</sup> However, no defects were observed in the surrounding area of region D. Therefore, self-interstitials are the dominant point defect existing in region D. In the surrounding area of region D, since a small amount of self-interstitials suppress the formation of oxygen precipitation nuclei, oxygen precipitation cannot occur even if the wafer is subjected to 2-step annealing. Therefore, the surrounding area of region D is a self-interstitial-type grown-in defect-free region.

#### 2.2.4. v/G Defect Map

To discuss the control method of grown-in defect-free crystals, hereafter we call the region A as Pv region and the peripheral area in region D as Pi region, where Pv or Pi means vacancy or self-interstitial dominated Pure region, respectively. In these regions, grown-in defects, such as voids and dislocation clusters, do not exist. However, oxygen-precipitation nuclei exist in the Pv region but do not in the Pi region. If we can fabricate only the Pv and/or Pi region over the entire area of the wafer, such a wafer would be preferable for device fabrication. Our goal was to develop a control technique to fabricate these defect-free regions for the entire length of the crystal. For this purpose, we studied how radial defect distribution relates to radial v/G distribution.

**Figure 6(a)–(d)**, respectively, show the radial distributions of v/G values calculated at axial positions of 100, 200, 300, 400 mm and other characteristic positions for all crystals, and the four defect regions are mapped by the closed or open squares in each figure. In the radial position from the center to about 45 mm, the v/G values on the boundaries of each defect region were almost constant, and the OSF-ring region was mapped near a critical value of v/G of about 0.22 mm<sup>2</sup> (°C min)<sup>-1</sup>. Region C inside the OSF-ring was mapped for values of v/G larger than the critical value. In the area of v/G smaller than the critical value, region D with dislocation clusters appeared on the v/G map.

**Figure 7** shows a schematic of the v/G map, which summarizes the four defect maps shown in Figure 6(a)–(d). This is considered a type of phase diagram showing the type of grown-in defects appearing in CZ-Si crystals as a function of v/G and crystal radial position. Generally, crystals are cooled at the outer periphery to maximize crystal productivity. Therefore, the temperature gradient for the outer side of the crystal is larger than that for the crystal center, so the v/G is smaller for the outer periphery, as shown with lines a)–c) for the conventional hot zone in Figure 7. When v was high, as shown with line a), most of the crystal was covered with a void area, and the OSF-ring

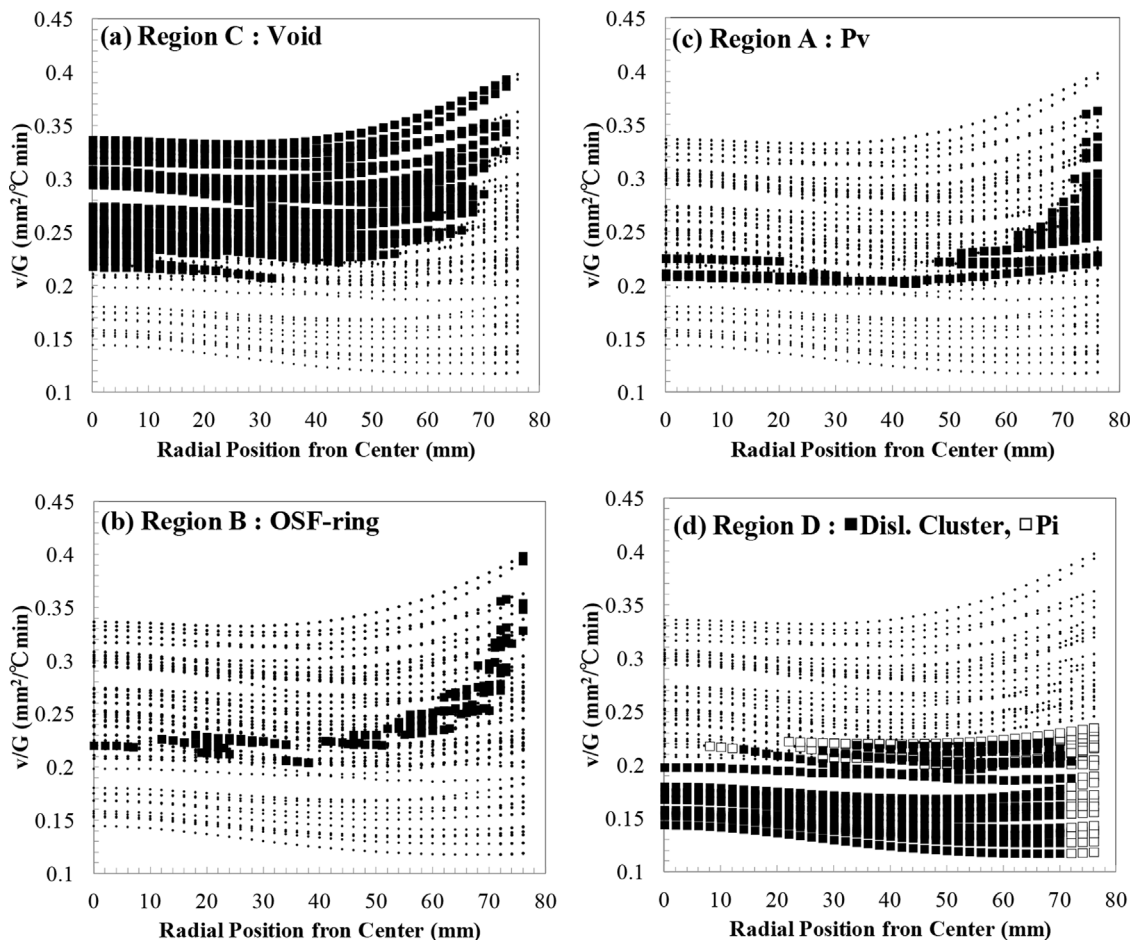


**Figure 6.** Calculated values of  $v/G$  shown with small dots at various positions for all crystals as function of radial position. Four defect regions mapped with closed or open squares can be clearly observed; (a) region C: void, (b) region B: OSF-ring, (c) region A: Pv, and (d) region D: dislocation cluster and Pi. Adapted with permission.<sup>[23]</sup> Copyright 1995, Trans Tech Publications Ltd.

appeared at the outer side of the crystal, as shown in pattern a). If  $v$  is reduced while maintaining similar  $G$  distribution, the  $v/G$  curve shifts downward, as shown with line b), so the OSF-ring as well as the void area shrink, and the dislocation clusters appear outside the OSF-ring, as shown in defect pattern b). Furthermore, if  $v$  is reduced further, as shown with line c), the OSF-ring disappears in the crystal center at the critical  $v/G$ , and dislocation clusters appear over the entire area of the crystal, as shown in defect pattern c).

#### 2.2.5. Growth Concept for Grown-In Defect Free Crystal

Line d) in Figure 7 schematically shows the growth concept for a grown-in defect-free crystal.<sup>[30,41]</sup> A narrow but perfectly defect-free area in the radial direction can be seen in the  $v/G$  map. If the  $G$  distribution can be made uniform in the radial direction and  $v/G$  can be maintained in the defect-free area by controlling the pulling rate during crystal growth, it may be possible to achieve the grown-in defect-free condition for the entire length of the crystal. Under this condition, the amount of

vacancies can be balanced with that of self-interstitials during crystal growth, so that the generation of grown-in defects can be suppressed.

From the experimental results explained in Section 2.2.2, a grown-in defect-free crystal was fabricated naturally without intentional effort, as shown in Figure 3(d). This crystal was grown with a pulling rate of  $0.4 \text{ mm min}^{-1}$  in hot zone IV with the smallest and most uniform radial  $G$  distribution. Region including dislocation clusters was observed up to about 250 mm from the top part of the crystal, but thereafter Pi and Pv-type grown-in defect-free regions were appeared over about 250 up to 550 mm, then the OSF-ring appeared.

We also conducted a test to verify the growth concept of  $v/G$  control to obtain a much longer grown-in defect-free crystal. We grew two crystals (diameter; 155 mm,  $<100>$ , B-dope p-type,  $120 \Omega \text{ cm}$ ) using a hot zone (crucible diameter; 18 inches, charge weight; 45 kg, shield-melt gap; 75 mm, melt position;  $-130 \text{ mm}$ ) with and without pulling rate control.<sup>[30,31]</sup> Figure 8 (a) shows X-ray topography images of a longitudinal section of the crystal grown at a constant pulling rate of  $0.4 \text{ mm min}^{-1}$  after 200 mm of the crystal length. At 200 mm, the OSF-ring

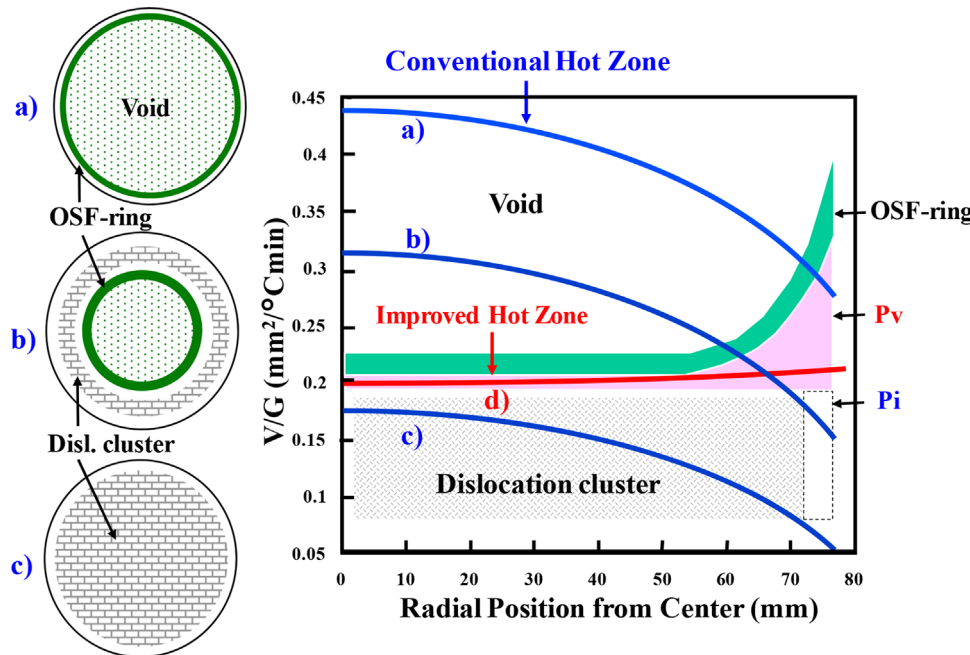


**Figure 7.** Schematics of  $v/G$  defect maps, which summarize four defect maps shown in Figure 6(a)–(d), defect pattern changes (a)–(c) with decreasing crystal pulling rate in conventional hot zone, and (d) growth concept for grown-in defect-free crystal by using improved hot zone. Adapted with permission.<sup>[30]</sup> Copyright 1998, Electrochemical Society.

disappeared and Pi- and Pv-type grown-in defect-free regions D and A appeared. The OSF-ring occurred again at the position of about 300 mm, and the ring diameter markedly increased almost over the entire area of the crystal at about 420 mm. This means that the radial distribution of point-defect concentration would be very uniform and the temperature gradient G would gradually decrease toward the crystal tail. Therefore, the pulling rate was adjusted, as shown in Figure 8(b), to maintain the critical condition for the Pi- and/or Pv-type grown-in defect-free states. With this operation, as shown in Figure 8(c), Pi-type grown-in defect-free region D appeared at the position from 200 to 300 mm, thereafter Pv-type grown-in defect-free region A continued for almost all the crystal length until the tail end. Grown-in defects, such as voids and dislocation clusters, were not observed in regions A and D by using an optical precipitate profiler (OPP) and Secco etching. We also examined the GOI characteristics on wafers cut from the crystal between 300 and 400 mm and confirmed that they are excellent and equivalent to epitaxial wafers, as shown in Figure 9.

After that, based on the concept of the  $v/G$  control, we have completed a mass-production technology for 200 and 300-mm grown-in defect-free crystals by applying a hot-zone design tool for uniform G distribution and new control technology to maintain an optimal thermal environment. We also developed a magnetic-field technology that enables optimization of oxygen concentration and growth interface shape and maximization of growth rate through controlling the melt convection.<sup>[4,5]</sup> Currently, 200 and 300-mm grown-in defect-free crystals have become standard for various devices because they can stably provide a huge amount of high-quality wafers at low cost.

### 3. Comment on Development of MCZ-Si Crystals for Future Silicon Power Devices

#### 3.1. MCZ-Si Wafers for IGBTs

The 21st century is the era of electric energy; thus, an enormous demand for electric energy and a rapid increase in electrification ratio, i.e., ratio of electric power consumption to total energy consumption, is expected on a global scale.<sup>[42,43]</sup> Power devices that can perform power conversion and switching with high efficiency are the core technology in power electronics. Therefore, the role and popularization of power devices will become more important. Recently, wide band gap semiconductor materials, such as SiC and GaN, have emerged in power electronics as next-generation materials to replace silicon. However, they have a large gap in their productivity and crystal perfection compared with silicon. Therefore, the role of silicon as a main material for power devices will remain, and silicon wafers with much higher quality at lower cost as well as ultimate silicon power devices must be developed.<sup>[42,44]</sup>

We developed 200-mm-diameter MCZ-Si wafers in 2008 for application to automotive IGBTs. Conventionally, thick epitaxial wafers of about 50–100  $\mu\text{m}$  have been used for medium-voltage (600 and 1200 V) IGBTs, but bulk wafers of 200 mm in diameter are required from the viewpoint of cost reduction and stable supply. In addition, high purity FZ-Si crystals have also been conventionally used for high-voltage devices such as diodes and IGBTs. However, at that time, manufacturers capable of supplying 200-mm-diameter FZ-Si crystals were limited, so we decided to develop extremely low-oxygen MCZ-Si wafers to replace FZ-Si wafers.

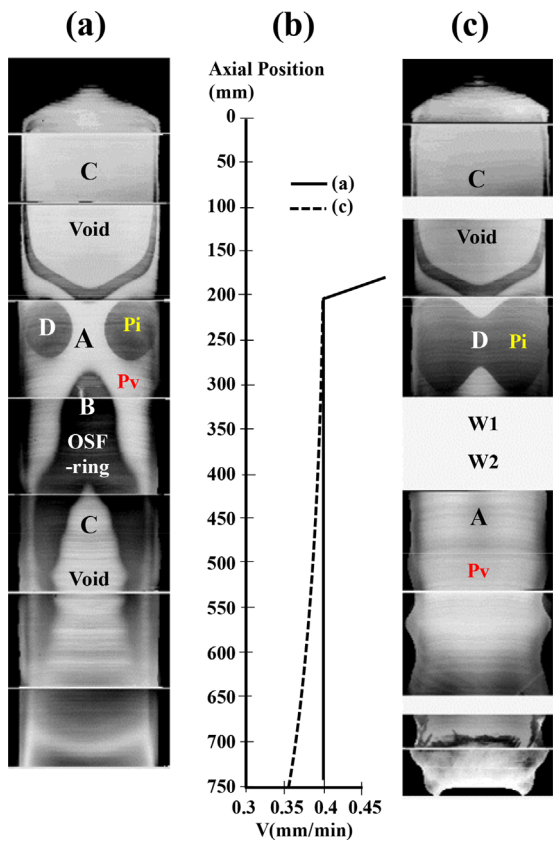


**Figure 8.** X-ray topography images of crystals grown at (a) constant pulling rate of  $0.4 \text{ mm min}^{-1}$ , (c) constant v/G around critical condition for grown-in defect-free state, and (b) crystal pulling rates to grow crystals in (a) and (c). Adapted with permission.<sup>[30]</sup> Copyright 1998, Electrochemical Society.

In the development process of MCZ-Si wafers for IGBTs, the following have been clarified as technical problems regarding crystal quality. (1) Voids degrade the gate-emitter (G-E) breakdown voltage of IGBTs, that is, the GOI characteristics of the MOS diode. (2) BMDs, such as oxygen precipitates, and their secondary defects, such as stacking faults and dislocation loops, degrade the lifetime characteristics of IGBTs; thus, increasing the collector-emitter (C-E) leakage current and on-voltage. (3) Resistivity changes due to oxygen donors degrade the C-E breakdown voltage. From the above, the requirements of crystal quality of MCZ-Si wafers applied to IGBTs were found to be extremely low oxygen concentration ( $\leq 6\text{E}17 \text{ atoms cm}^{-3}$ ), void free, and BMD free.

When we began developing 200-mm-diameter MCZ-Si wafers, we first tried to apply the growth technology of grown-in defect-free crystals by v/G control. However, crystals with simultaneous void-free and very low oxygen concentration were difficult in the as-grown state. For this reason, we developed an oxygen-annealing technique to annihilate voids in the bulk of MCZ-Si wafers at high temperature, with which a thin oxide film on the inner wall of a void is first dissolved by under-saturation of oxygen concentration then the void is filled with self-interstitials injected by oxidation.<sup>[45]</sup> However, voids near the surface region remain; thus, they need to be removed by deep polishing. Such high-temperature annealing and deep polishing are costly processes and allow for unintentional contamination such as by metals and other impurities. Therefore, current MCZ-Si wafers for IGBTs still have much room to be improved.

The application of 300-mm silicon wafers to silicon power devices has recently been promoted in Europe. However, since it would be very difficult to develop growth technology of 300-mm FZ-Si crystal growth, 300-mm MCZ-Si crystals will be as the main material for future Si power devices. Therefore, it is necessary to develop 300-mm MCZ-Si wafers with higher quality at lower cost. As candidate techniques to fabricate 300-mm MCZ-Si crystals, we propose nitrogen doping and hydrogen doping with v/G control during crystal growth.

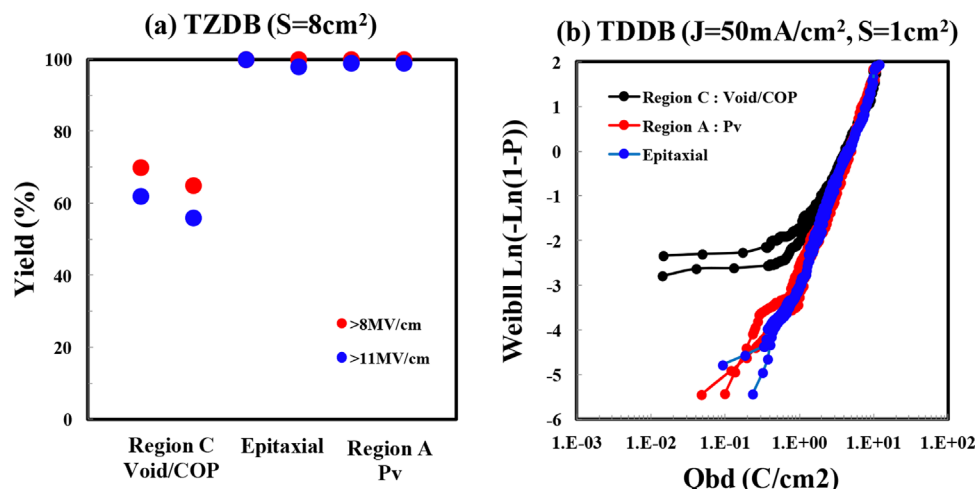


**Figure 9.** GOI characteristics of (a) time zero dielectric breakdown (TZDB) and (b) time-dependent dielectric breakdown (TDDB) examined on wafers W1 and W2 shown in Figure 8(c) compared with wafers from region C and epitaxial wafers. S: gate area of MOS diode, J: current density, Qbd: charge-to-breakdown.

### 3.2. Nitrogen-Doped CZ-Si Crystals

It was reported by Abe that nitrogen-gas doping into FZ-Si crystals during growth suppresses the generation of D and A defects.<sup>[46,47]</sup> It is also well known that if FZ-Si crystals are not doped with nitrogen, voids occur similarly to CZ-Si crystals.<sup>[48,49]</sup> However, FZ-Si crystals, which are supplied on a commercial basis, are substantially void free as they are doped with nitrogen.<sup>[50]</sup>

Figure 10 shows the change in defect states in a 150-mm-diameter CZ-Si crystal doped with nitrogen gas during crystal growth. Nitrogen gas was mixed in argon atmosphere at 400-mm position of the crystal's length during growth at a pulling rate of  $0.7 \text{ mm min}^{-1}$ . Nitrogen gas dissolves into silicon melt, then nitrogen is introduced from the melt into the crystal by segregation. As in the case of a FZ-Si crystal, void generation is suppressed, but the OSF-ring spreads throughout the crystal. A similar phenomenon has been reported by Nakai et al., Iida et al., and Nakamura et al., and the effect of nitrogen on voids or the OSF-ring was discussed by using reaction models of complexes between nitrogen, oxygen, and point defects.<sup>[51–53]</sup>

Figure 11 shows a schematic of a v/G map for a nitrogen-doped CZ-Si crystal as a function of nitrogen concentration. Iida et al.<sup>[52]</sup> reported defect behavior in nitrogen-doped CZ-Si crystals with high oxygen concentration of  $12\text{E}17 \text{ atoms cm}^{-3}$  and low oxygen concentration of  $5.5\text{E}17 \text{ atoms cm}^{-3}$ . In the case of high oxygen concentration, the v/G range for the OSF-ring region markedly enlarged in the range of the nitrogen concentration from  $1\text{E}13$  to  $1\text{E}15 \text{ atoms cm}^{-3}$ . In the case of low oxygen concentration, however, OSFs did not occur and the OSF-ring region turned into a Pv-type grown-in defect-free region. Therefore, if MCZ-Si crystals with low oxygen concentration of about  $5\text{E}17 \text{ atoms cm}^{-3}$  or lower are doped with nitrogen, Pv-type grown-in defect-free wafers can be fabricated. However, it was also reported that in spite of such low oxygen concentration, BMDs with low densities of  $1\text{E}6$ – $1\text{E}7 \text{ cm}^{-3}$  generate in such Pv-type grown-in defect-free wafers. If such a low density of BMDs does not affect the device characteristics of IGBTs, the Pv-type grown-in defect-free wafers obtained from nitrogen-doped MCZ-Si crystals can be used as substrates for future IGBTs. When nitrogen is doped into a CZ-Si crystal, however the nitrogen concentration varies depending on the solidification ratio of the crystal due to impurity segregation during solidification, so that the BMD density would vary depending on the position of the crystal. Therefore, it is necessary to clarify appropriate ranges of nitrogen and oxygen

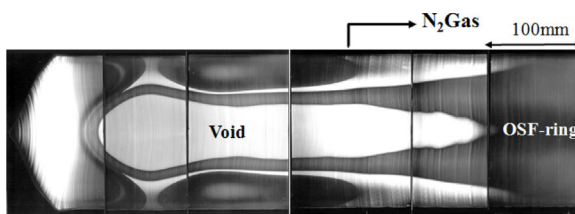


**Figure 10.** X-ray topography image taken after 2-step annealing of crystal doped with nitrogen gas during crystal growth.

concentrations that do not affect the device characteristics of IGBTs.

### 3.3. Hydrogen-Doped CZ-Si Crystals

We developed hydrogen-doped CZ-Si crystal technology in 2005 to increase process window of the v/G control for grown-in defect-free crystals.<sup>[54,55]</sup> Hydrogen can be doped into a CZ-Si crystal through silicon melt by mixing hydrogen gas in argon atmosphere at a concentration range of up to 8% during crystal growth. If argon gas with a certain constant concentration of hydrogen flows into a CZ furnace at a constant flow rate, a steady state of hydrogen concentrations between the silicon melt and argon atmosphere would be maintained, so that hydrogen concentration in the silicon melt can be kept constant. Therefore, the concentration of hydrogen in the crystal also can be kept constant from the top to bottom of the crystal. Moreover, the hydrogen concentration in the crystal can be controlled by changing the hydrogen concentration in the argon atmosphere.

From the viewpoint of safe operation, we needed to determine the upper limit of hydrogen concentration in the argon atmosphere. Generally, a CZ furnace is operated under reduced pressure. Assuming the case in which the furnace is accidentally opened to atmosphere and air flows into the furnace, in the ternary system between argon, atmospheric air, and hydrogen, we conducted safety engineering experiments to study hydrogen combustion and detonation, and the upper limit of safe hydrogen concentration with no hydrogen combustion was confirmed to be 10%. Therefore, we determined the upper limit of hydrogen concentration in argon atmosphere to be 8% for a safe operation of a CZ furnace.

Five hydrogen-doped CZ-Si crystals with a diameter of 150 mm were grown using a hot zone with uniform G distribution while reducing the pulling rate from 0.6 to  $0.3 \text{ mm min}^{-1}$ . For the growth of each crystal, hydrogen gas was mixed in argon atmosphere at concentrations of 0, 2, 4, 6, and 8%. The crystal was cut longitudinally and an X-ray topography images after 2-step annealing were taken. Figure 12 shows the case in which the hydrogen concentrations were 0 and 6% for comparison. Although the Pv-type grown-in defect-free

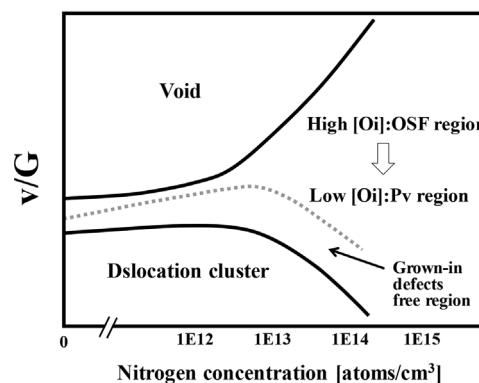


**Figure 11.** Schematic of v/G defect map for nitrogen-doped CZ-Si crystal as function of nitrogen concentration.

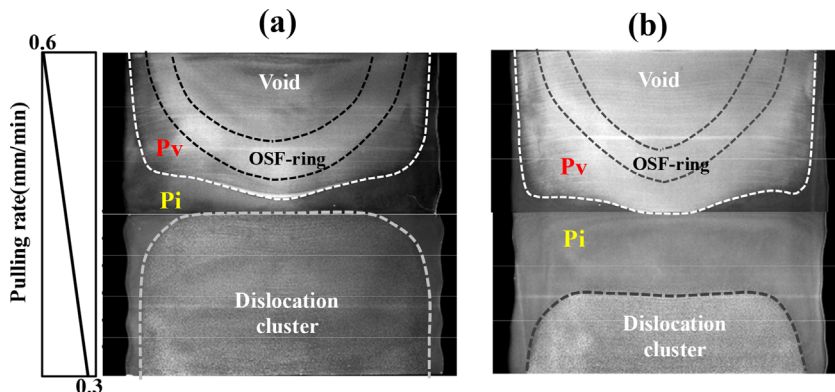


**Figure 12.** X-ray topography images of grow-in defect distribution after 2-step annealing for crystals doped with hydrogen concentrations of (a) 0 and (b) 6%, respectively. Adapted with permission.<sup>[54]</sup> Copyright 2014, National Diet Library.

margin did not change much, the Pi-type grown-in defect-free margin expanded markedly. **Figure 13** shows the v/G defect map for the hydrogen-doped CZ-Si crystal as a function of hydrogen concentration. It was found that the Pi-type v/G region expanded to the low v/G side as the hydrogen concentration increased. This indicates that hydrogen atoms hardly interact with vacancies during crystal growth at high temperatures around 1100 °C at which voids are generated, but they can interact with self-interstitials at a much lower temperature of 950 °C, effectively suppressing the formation of dislocation clusters.<sup>[37,56]</sup> Therefore, Pi-type grown-in defect-free wafers can be fabricated by hydrogen doping in the CZ-Si crystals.

**Figure 14** shows an example of examining the oxygen-precipitation behavior of a 300-mm-diameter grown-in defect-free CZ-Si crystal grown using hydrogen-doping technique combined with v/G control. The grown crystal was B-dope, with a resistivity of 11.2–9.1 Ω cm, and oxygen concentration of

12.9–10.0 E17 atoms cm<sup>-3</sup>. After dividing these wafers into four parts, etched pits due to BMDs after 2 min of Wright etching were counted with a microscope after 2-step annealing at  $T$  °C/4 h + 1000 °C/16 h, where  $T$  is 700, 800, or 900, and 1-step annealing at 1000 and 1100 °C/16 h. **Figure 13(a)** shows the case of the 300-mm wafer in which Pi and Pv regions coexist, and **Figure 13(b)** shows the 300-mm wafer with only the Pi region. Although BMDs were observed in the Pv region, no BMDs were observed in the Pi region. From these facts, it can be said that Pi-type wafers completely free of BMDs as well as voids can be fabricated from hydrogen-doped MCZ-Si crystals with extremely low oxygen concentration grown with v/G control. Since these wafers are considered to have crystal quality equivalent to FZ-Si wafers, they are expected to be used as high quality and low-cost wafers suitable for future IGBTs.

It is necessary to mention the disadvantages regarding hydrogen-doped MCZ-Si crystals. One disadvantage concerns safety, such as combustion and explosion of hydrogen gas during crystal growth, and the other is concerned with the occurrence of characteristic hydrogen defects in the crystals.<sup>[54]</sup> It was already mentioned that it is possible to avoid the former problem by setting the upper limit of hydrogen gas concentration into the CZ furnace. Since hydrogen is contained in exhaust products, such as SiO dust, in the CZ process, there is another safety issue of an increase in the combustibility and explosiveness of SiO dust. To solve this problem, it is necessary for a process to gradually burn the exhaust products without suddenly exposing them to the atmospheric air.

Hydrogen defects have been studied in detail by Sugimura et al.<sup>[54]</sup> The nature of such defects is a crack with its origin confirmed to be voids and dislocation clusters. For this reason, hydrogen defects occur in the void and dislocation-cluster regions but not in the Pv, Pi, and OSF-ring regions. From a rapid crystal detaching and quenching experiment, the formation temperature of hydrogen defects was found to be 680 °C, which is lower than the formation temperatures of voids and dislocation clusters, i.e., 1100 and 950 °C, respectively.<sup>[37,56]</sup> Therefore, after formation of voids and dislocation clusters, super-saturated hydrogen atoms agglomerate on the (100) or (111) plane at those defects as a starting point, so that the covalent bonding force of silicon decreases, then cracks occur

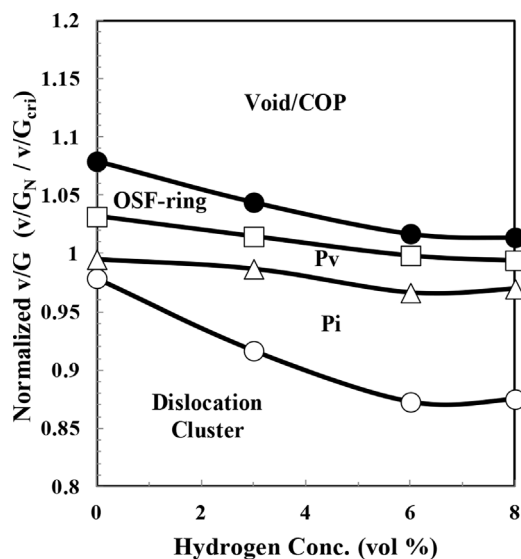


**Figure 13.** Normalized v/G defect map of hydrogen-doped CZ-Si crystals as function of hydrogen concentration in argon atmosphere during crystal growth. Adapted with permission.<sup>[54]</sup> Copyright 2014, National Diet Library.

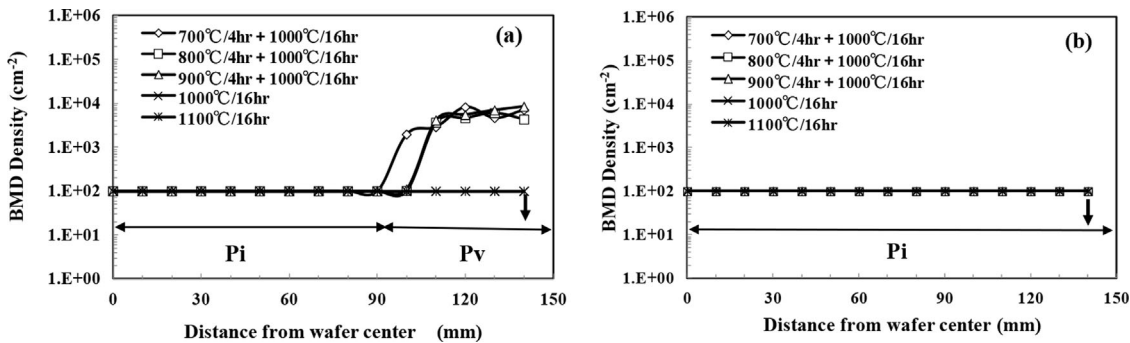


**Figure 14.** BMD density distributions after various heat conditions of 300-mm CZ-Si wafers with (a) Pv and Pi grown-in defect-free regions and  $[O_i] = 10.1E17 \text{ cm}^{-3}$  and (b) Pi defect-free region and  $[O_i] = 11.0E \text{ cm}^{-3}$ , which were cut from crystal grown using hydrogen-doping technology combined with v/G control. Arrows in (a) and (b) show detection limits.

due to an external stress during crystal growth. Since hydrogen defects are huge disk-shaped cracks having a diameter of 10–20  $\mu\text{m}$ , they can be easily detected using a defect-detection tool such as a laser particle counter. Therefore, it is possible to screen wafers containing hydrogen defects. Through such inspection, 10 000 pieces of 300-mm grown-in defect-free hydrogen-doped wafers without hydrogen defects were put into advanced memory devices at that time around 2005. It was verified that the device characteristics and yield are equivalent to those of ordinary grown-in defect-free wafers without hydrogen doping.

### 3.4. Future Research

To make the conductivity modulation on IGBTs more effective, it is necessary to keep the carrier lifetime high to increase the breakdown voltage and reduce the on-voltage and conduction loss of bipolar-type power devices such as IGBTs. To improve the switching speed and suppress switching loss, it is also necessary to control the carrier lifetime. For some devices, such as a reverse-conducting IGBT, lifetime control has been carried out by irradiation with charged particles such as electron beams or protons. However, due to the evolution of IGBTs, lifetime control has not been required in modern IGBTs such as a punch-through-type or field-stop-type IGBTs, so it is generally required to maintain as high a carrier lifetime as possible.

Since quartz crucibles and carbon parts are used for CZ-Si crystal growth, impurities, such as oxygen and carbon, are introduced into the crystals. Defects, such as oxygen precipitates and vacancy-light element complexes, form due to the interaction between these impurities and point defects during device processes, such as ion implantation, so that they would degrade carrier lifetime and increase C-E leakage current and on-voltage of IGBTs. It has recently been reported that carbon-related complexes, such as Ci-Cs (G-line) and Ci-Oi (C-line), decrease lifetime.<sup>[57–59]</sup> Therefore, reducing carbon in the crystal has been required. In addition, because high-voltage IGBTs for infrastructure applications of a power supply require high resistivity and high lifetime materials, FZ-Si crystals with neutron transmutation doping (NTD) are used. This is presumed to be due to the fact that carbon, oxygen, or dopant impurities in the crystal forming complexes with point defects

introduced by NTD or ion implantation during device processes. However, it is not well understood what types of defects are generated and how they affect carrier lifetime.

Finally, to maximize performance of all types of power devices not only limited to IGBTs, silicon crystals will be required to pursue their quality limitations, for example, much lower resistivity and higher crystal perfection for low-voltage power MOS devices, more uniform high resistivity, and much higher purity and carrier lifetime for high-voltage IGBTs. Such challenges to pursue the crystal quality limitations for silicon power devices frequently provide unexpected and interesting physical phenomenon. Therefore, we believe that the technical issues mentioned above must be addressed as research subjects common to academia and device and wafer manufacturers.

## 4. Conclusion

We investigated the detailed distributions of grown-in defects and temperature in many CZ-Si crystals grown with different pulling rates and hot zones to change the thermal environment in crystals. The position of the OSF-ring was normalized without depending on the hot zones by v/G, and the OSF-ring shrunk and disappeared at a certain critical v/G. We thus concluded that the type of grown-in defects in the CZ-Si crystal is determined by v/G. We also created a v/G defect map by analyzing the relationship between radial distributions of various defects and v/G values at corresponding positions. This map is a type of phase diagram showing the type of grown-in defects appearing in CZ-Si crystals as a function of v/G and crystal radial position. In this map, there is a narrow but perfectly defect-free v/G window without voids and dislocation clusters throughout the crystal radial direction. We thus developed the growth concept for grown-in defect-free crystals over the entire length and verified it with a 150-mm-diameter CZ crystal. This concept was then applied to the mass production of 200- and 300-mm grown-in defect-free CZ-Si crystals, which have become standard crystals used for various devices.

We have developed very low oxygen 200-mm MCZ-Si wafers for IGBTs for automotive use. However, it was difficult to make them be grown-in defect free as well as low oxygen simultaneously in as-grown state; therefore, they contain voids that must be annihilated by high-temperature oxygen annealing.

To develop 300-mm MCZ-Si wafers with higher quality at lower cost for future IGBTs, we proposed nitrogen- and hydrogen-doping techniques for fabricating grown-in defect-free MCZ-Si crystals with very low oxygen in the as-grown state. It is possible to expand the process window for grown-in defect-free crystals by combining nitrogen doping or hydrogen doping with v/G control. In the case of nitrogen doping, Pv-type defect-free crystals, which are dominated by vacancy can be obtained and oxygen precipitation can be enhanced even if oxygen is very low. In the case of hydrogen doping, Pi-type defect-free crystals, which are dominated by self-interstitials, can be obtained and would be preferable for future IGBTs because they would be free of oxygen precipitates as well as voids. However, we currently do not know which type of crystal is the most suitable for future IGBTs and what specifications, such as BMD, concentrations of oxygen and other elements such as carbon, should be satisfied for higher performance of future IGBTs. Therefore, these technical issues must be addressed as research subjects common to academia and device and wafer manufacturers.

## Conflict of Interest

The authors declare no conflict of interest.

## Keywords

grown-in defects, hydrogen doping, point defects, power device, silicon

Received: August 21, 2018

Revised: October 22, 2018

Published online:

- [1] H. R. Huff, *J. Electrochem. Soc.* **2002**, *149*, 535.
- [2] H. Tsuya, *Jpn. J. Appl. Phys.* **2004**, *43*, 4055.
- [3] T. Abe, *Oyo Buturi* **2007**, *76*, 927.
- [4] H. Furuya, in *7th International Symposium on Advanced Science and Technology of Silicon Materials 2016*, Hawaii, USA, Nov. **2016**, p. 1.
- [5] H. Furuya, in *29th International Conference on Defects in Semiconductors*, Matsue, Japan, July–Aug. **2017**, MoPL1.
- [6] M. Hasebe, Y. Takeoka, S. Shinomiya, S. Naito, *Jpn. J. Appl. Phys.* **1989**, *26*, L1999.
- [7] H. Tachimori, T. Sakon, T. Kaneko, 7th Kessho Kougaku Symposium of Japan Soc. of Appl. phys. (JSAP Catalog No.: 902217), **1990**, p. 27.
- [8] P. Gall, J. P. Fillard, J. Bonnafé, T. Rakotomovo, H. Rufer, H. Schwenk, in *Defect Control in Semiconductors* (Ed: K. Sumino), North-Holland, Elsevier Science Publishers B.V., Amsterdam, the Netherlands **1989**, p. 255.
- [9] S. Sadamitsu, S. Umeno, Y. Koike, M. Hourai, S. Sumita, T. Shigematsu, *Jpn. J. Appl. Phys.* **1993**, *32*, 3675.
- [10] H. Yamagishi, I. Fusegawa, N. Fujimaki, M. Katayama, *Semicond. Sci. Technol.* **1992**, *7*, A135.
- [11] J. Ryuta, E. Morita, T. Tanaka, Y. Shimanuki, *Jpn. J. Appl. Phys.* **1990**, *29*, L1947.
- [12] M. Hourai, M. Sano, S. Sumita, T. Shigematsu, in *Progress in Semiconductor Fabrication, SEMICON/Europa'93 Technical Conference*, Geneva, March/April, **1993**.
- [13] K. Takano, K. Kitagawa, E. Iino, M. Kimura, H. Yamagishi, in *Materials Science Forum*, Vol. 196–201, *Defect in Semiconductor 18*, (Eds: M. Suezawa, H. Katayama-Yoshida), Trans Tech Publications, Zurich-Uetikon, Switzerland **1995**, p. 1707.
- [14] E. Dornberger, W. von Ammon, D. Graf, U. Lambert, A. Miller, H. Oelkrug, A. Ehlert, in *High Purity Silicon IV, PV 96-13* (Eds: C. L. Claeys, P. Rai-Choudhury, P. Stallhofer, J. E. Mautis), Electrochem. Soc., Pennington, NJ., USA **1996**, p. 140.
- [15] S. Umeno, M. Okui, M. Hourai, M. Sano, H. Tsuya, *Jpn. J. Appl. Phys.* **1997**, *36*, L591.
- [16] M. Kato, Y. Ikeda, Y. Kitagawara, *Jpn. J. Appl. Phys.* **1996**, *35*, 5597.
- [17] M. Nishimura, S. Yoshino, M. Motoura, S. Shimura, T. Mchedlidze, T. Hikono, *J. Electrochem. Soc.* **1996**, *143*, L243.
- [18] T. Ueki, M. Itsumi, T. Takeda, *Appl. Phys. Lett.* **1997**, *70*, 1248.
- [19] H. Yamamoto, H. Koyama, in *Proc. 2nd Int. Symp. Advanced Science and Tech. of Silicon Materials* (Ed: M. Umeno), Kona-Hawaii, USA, Nov. **1996**, p. 425.
- [20] F. Gonzalez, G. A. Rozgonyi, B. Gilgen, R. Barbour, in *High Purity Silicon IV, PV 96-13* (Eds: C. L. Claeys, P. Rai-Choudhury, P. Stallhofer, J. E. Mautis), Electrochem. Soc., Pennington, NJ., USA **1996**, p. P357.
- [21] P. J. Roksnoer, M. M. B. van den Boom, *J. Cryst. Growth* **1981**, *53*, 563.
- [22] V. V. Voronkov, *J. Crystal Growth* **1982**, *59*, 625.
- [23] M. Hourai, E. Kajita, T. Nagashima, H. Fujiwara, S. Umeno, S. Sadamitsu, S. Miki, T. Shigematsu, in *Materials Science Forum*, Vol. 196–201, *Defect in Semiconductor 18* (Eds: M. Suezawa, H. Katayama-Yoshida), Trans Tech Publications, Zurich-Uetikon, Switzerland **1995**, p. 1713.
- [24] S. Miyahara, S. Kobayashi, T. Fujiwara, T. Kubo, H. Fujiwara, in *Semiconductor Silicon 1990, PV 90-7* (Eds: H. R. Huff, K. G. Barraclough, J. Chiwawa), Electrochem. Soc., Pennington, NJ., USA **1990**, p. 94.
- [25] E. Kajita, M. Hourai, H. Fujiwara, S. Miki, T. Shigematsu, Extended Abstracts (The 42nd Spring Meeting, **1995**); The Japan Society of Applied Physics and Related Societies, 28a-ZW-3.
- [26] W. von Amon, E. Dornberger, H. Oelkrug, H. Weidner, *J. Cryst. Growth* **1995**, *151*, 273.
- [27] R. A. Brown, D. Maroudas, T. Sinno, *J. Crystal Growth* **1994**, *137*, 12.
- [28] K. Nakamura, T. Saishoji, T. Kubota, T. Iida, Y. Shimanuki, T. Kotooka, J. Tomioka, *J. Crystal Growth* **1997**, *180*, 61.
- [29] N. Ono, K. Harada, J. Furukawa, K. Shimanuki, M. Kida, Y. Shimanuki, in *Semiconductor Silicon 1998, PV 98-1* (Eds: H. R. Huff, U. Gösele, H. Tsuya), Electrochem. Soc., Pennington, NJ., USA **1998**, p. 503.
- [30] M. Hourai, H. Nishikawa, T. Tanaka, S. Umeno, E. Asayama, T. Nomachi, G. Kelly, in *Semiconductor Silicon 1998, PV 98-1* (Eds: H. R. Huff, U. Gösele, H. Tsuya), Electrochem. Soc., Pennington, NJ., USA **1998**, p. 453.
- [31] M. Hourai, H. Nishikawa, T. Tanaka, K. Nomachi, E. Asayama, S. Umeno, *J. Jpn. Assoc. Cryst. Growth* **1998**, *25*, 207.
- [32] R. Habu, I. Yunoki, T. Saio, *Jpn. J. Appl. Phys.* **1993**, *32*, 1740.
- [33] R. Habu, T. Iwasaki, H. Harada, A. Tomiura, *Jpn. J. Appl. Phys.* **1993**, *32*, 1747.
- [34] R. Habu, K. Kojima, H. Haraga, A. Tomiura, *Jpn. J. Appl. Phys.* **1993**, *32*, 1754.
- [35] R. Habu, I. Yunoki, T. Saio, *Jpn. J. Appl. Phys.* **1996**, *35*, 1.
- [36] M. Hourai, T. Nagashima, E. Kajita, S. Miki, S. Sumita, S. Sano, T. Shigematsu, in *Semiconductor Silicon 1994, PV94-10* (Eds: H. R. Huff, W. Bergholz, K. Sumino) Electrochem. Soc., Pennington, NJ., USA **1994**, p. 156.
- [37] H. Nisikawa, T. Tanaka, Y. Yanase, M. Hourai, M. Sano, H. Tsuya, *Jpn. J. Appl. Phys.* **1997**, *36*, 6595.
- [38] M. Hourai, T. Nagashima, E. Kajita, S. Miki, T. Shigematsu, M. Okui, *J. Electrochem. Soc.* **1995**, *142*, 3193.

- [39] K. Marsden, S. Sadamitsu, M. Hourai, S. Sumita, T. Shigematsu, *J. Electrochem. Soc.* **1995**, 142, 996.
- [40] T. Kanda, K. Marsden, M. Hourai, S. Miki, T. Shigematsu, H. Tomokage, Extended Abstracts (The 42nd Spring Meeting, 1995); The Japan Society of Applied Physics and Related Societies, 28a-ZW-2.
- [41] M. Hourai, E. Kajita (Sumitomo Mitsubishi Silicon Corp.), *Japan, JP 358724, B2*, 2004.
- [42] T. Hiramoto, I. Omura, *Oyo Buturi* **2017**, 86, 956.
- [43] <http://www.iea.org/etp/etp2014/>.
- [44] M. Tanaka, I. Omura, *Solid-State Electron.* **2013**, 80, 118.
- [45] S. Umeno, Y. Yanase, M. Hourai, M. Sano, Y. Shida, H. Tsuya, *Jpn. J. Appl. Phys.* **1999**, 38, 5725.
- [46] T. Abe, T. Masui, H. Harada, J. Chikawa, in *VLSI Science and Technology 1985, PV 85-5* (Eds: W. M. Bullis, S. Broydo), Electrochem. Soc., Pennington, NJ., USA **1985**, p. 543.
- [47] T. Abe, *J. Cryst. Growth* **2011**, 327, 1.
- [48] T. Saishoji, K. Nakamura, H. Nakajima, T. Yokoyama, F. Ishikawa, J. Tomioka, in *High Purity Silicon V, PV 98-13* (Eds: C. L. Claeys, P. Rai-Choudhury, M. Watanabe, P. Stallhofer, H. J. Dawson), Electrochem. Soc., Pennington, NJ, USA **1998**, p28.
- [49] M. Nishimura, Y. Yamaguchi, K. Nakamura, J. Jablonski, M. Watanabe, in *High Purity Silicon V, PV 98-13* (Eds: C. L. Claeys, P. Rai-Choudhury, M. Watanabe, P. Stallhofer,
- H. J. Dawson), Electrochem. Soc., Pennington, NJ., USA **1998**, p. 188.
- [50] T. Abe, *J. Cryst. Growth* **2011**, 334, 4.
- [51] K. Nakai, Y. Inoue, H. Yokota, A. Ikari, J. Takahashi, A. Tachikawa, K. Kitahara, Y. Ohta, W. Ohashi, *J. Appl. Phys.* **2001**, 89, 4301.
- [52] M. Iida, W. Kusaki, M. Tamatsuka, E. Iino, M. Kimura, S. Muraoka, in *Defect in Silicon III, PV 99-1* (Eds: T. Abe, W. M. Bullis, S. Kobayashi, W. Lin, P. Wagner), Electrochem. Soc., Pennington, NJ, USA **1999**, p. 499.
- [53] K. Nakamura, T. Saishoji, S. Togawa, J. Tomioka, in Proceedings of the Forum on the Science and Technology of Silicon Materials 2001 (Eds: H. Yamada-Kaneta, K. Sumino) Shonan, Kanagawa, Japan, Nov. **2001**, p. 109.
- [54] W. Sugimura, T. Ono, K. Nakamura, M. Hourai, K. Higashida, in Proceedings of the Forum on the Science and Technology of Silicon Materials 2014 (Eds: Y. Yoshida, H. Yamada-Kaneta), Hamamatsu, Japan, Oct., **2014**, p. 248.
- [55] M. Hourai, W. Sugimura, T. Ono (SUMCO Corp.) *Japan, JP 5023451, B2*, 2012.
- [56] M. Okui, T. Tanaka, T. Kanda, T. Ono, *Oyo Buturi* **1997**, 66, 707.
- [57] S. Nakagawa, K. Kashima, *Phys. Status Solidi C* **2014**, 11, 1597.
- [58] M. Tajima, H. Kiuchi, F. Higuchi, A. Ogura, *Appl. Phys. Express* **2017**, 10, 046602.
- [59] M. Tajima, Y. Ishikawa, H. Kiuchi, A. Ogura, *Appl. Phys. Express* **2018**, 11, 041301.